

# Space-time symmetry breaking in nonequilibrium frustrated magnetism

Mingxi Yue<sup>1</sup> and Zi Cai<sup>1,2,\*</sup>

<sup>1</sup>*Wilczek Quantum Center and Key Laboratory of Artificial Structures and Quantum Control, School of Physics and Astronomy, Shanghai Jiao Tong University, Shanghai 200240, China*

<sup>2</sup>*Shanghai Research Center for Quantum Sciences, Shanghai 201315, China*

 (Received 2 October 2022; revised 3 January 2023; accepted 13 February 2023; published 28 March 2023)

Spontaneous symmetry breaking is responsible for rich phenomena in equilibrium physics. Driving a system out-of-equilibrium can significantly enrich the possibility of spontaneous symmetry breaking, which occurs not only in space, but also in the time domain. This study investigates a driven-dissipative frustrated magnetic system with alternate ferromagnetic and antiferromagnetic coupling. Results show that frustration in such a far-from-equilibrium system could lead to nonequilibrium phases with intriguing space-time symmetry breaking, e.g., a discrete time crystal accompanied by a time-dependent magnetism with alternating tripartite stripe and ferromagnetic orders.

DOI: [10.1103/PhysRevB.107.094313](https://doi.org/10.1103/PhysRevB.107.094313)

## I. INTRODUCTION

Frustration arises when interaction energies cannot be simultaneously minimized for all bonds in a many-body system. It hosts remarkable phenomena ranging from a classical spin glass [1] to quantum spin liquids [2]. Typically, frustration may lead to macroscopic degeneracy in the classical ground-state manifold. However, this degeneracy could be lifted by thermal or quantum fluctuations, which may select particular configurations out of the degenerate manifold [3–5] or make a superposition among them to form exotic quantum states [6]. For the past decades, frustrated systems have been one of the central themes in condensed matter physics. However, with a few exceptions [7–11], most studies have restricted their the scope within equilibrium physics, which is governed by the paradigm of (free) energy minimization. The effect of frustration on nonequilibrium systems is far from clear, because these systems can absorb energy from outside, and thus are usually far from the ground state and the energy minimization principle does not necessarily apply.

Nonequilibrium physics is richer, albeit less known compared to equilibrium ones. An example is the spontaneous symmetry breaking (SSB), which plays a crucial role in both equilibrium and nonequilibrium systems. In contrast to thermal equilibrium SSB rooted in the variational principle of (free) energy minimization, the spatiotemporal patterns spontaneously emerging from nonequilibrium systems can only be understood within a dynamical framework, even for the steady state [12]. The nonequilibrium phases of matter differ from the equilibrium ones in the sense that the time dimension plays an equally, if not more, important role than the spatial dimensions in the classification of phases of matter. For instance, incorporating the time direction enriches the possibility of SSB, giving rise to interesting nonequilibrium

phases, like the time crystal that spontaneously breaks the time translational symmetry [13–33]. Frustration is a source of the exotic phase in equilibrium physics; thus, one may wonder whether it could lead to novel phases of matter in far-from-equilibrium systems.

In this study, we address this question by focusing on a driven-dissipative interacting spin model. Periodic driving usually heats a generic closed interacting system toward an infinite-temperature state. To avoid this featureless final state, we introduce dissipation by coupling each spin to a heat bath, which will drive the system to thermal equilibrium in the absence of periodic driving, as shown in the Appendix. Considering the notorious difficulty of dealing with quantum many-body dynamics, we focus on a classical system that enables us to simulate systems with dimension other than one up to a large system size. It has been shown that the exotic nonequilibrium phases are not restricted to quantum systems (e.g., the time crystal phases in classical many-body systems have recently been investigated [34–40]). Different from previous studies about the prethermal dynamics of close systems [10,39,40], here we focus on the long-time asymptotic behavior of the driven-dissipative system, and show that incorporating frustration enriches the categories of nonequilibrium phases of matter, and leads to magnetic states with intriguing space-time symmetry breaking.

## II. MODEL AND METHOD

We start with a two-dimensional classical spin model. The system Hamiltonian reads

$$H_s = H_0 + \lambda H_f, \quad (1)$$

where  $H_0$  is a frustration-free Hamiltonian (transverse Ising model) defined in a  $L \times L$  square lattice:

$$H_0(t) = V(t) \sum_{(ij)} s_i^x s_j^x - \sum_i h_z s_i^z, \quad (2)$$

\*zcai@sju.edu.cn

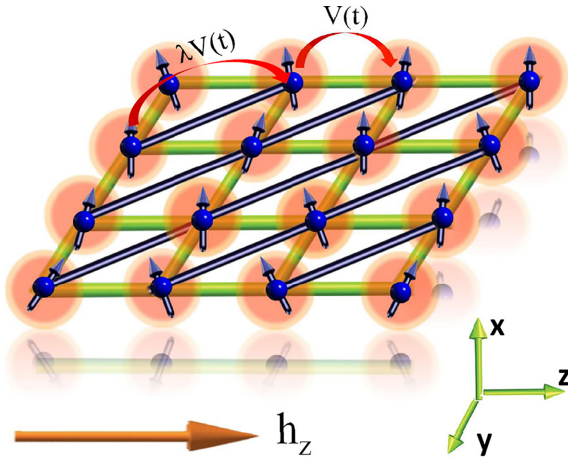


FIG. 1. Sketch of a driven-dissipative magnetic system in square lattice with next-nearest-neighbor coupling (blue bonds).

where the dynamical variable  $\mathbf{s}_i$  is a three-dimensional classical vector with a fixed length  $|\mathbf{s}_i| = 1$ , and the summation of  $\langle ij \rangle$  is over the two adjacent sites in the square lattice (green bonds; Fig. 1).  $h_z$  is the strength of the transverse field. Periodic driving  $V(t) = J + J' \cos \omega t$  is imposed on the interaction strength instead of the external field.  $V(t)$  can be either positive or negative, corresponding to antiferromagnetic (AFM) or ferromagnetic (FM) coupling. In our setup, alternate FM and AFM couplings during the time evolution is crucial. The frustration is introduced via the Hamiltonian  $H_f$ , whose strength is characterized by a dimensionless parameter  $\lambda$ . The frustration interaction is defined on one diagonal of each plaquette (blue bonds, Fig. 1). The Hamiltonian  $H_f$  reads

$$H_f(t) = V(t) \sum_{\langle\langle ij \rangle\rangle} s_i^x s_j^x. \quad (3)$$

Only one diagonal of each plaquette is included because in the undriven case ( $J' = 0$ ) with  $\lambda = 1$ , the Hamiltonian (1) is reduced to an AFM model defined on a triangle lattice, a prototypical example of frustrated magnetism. Throughout this paper, we assume  $J > 0$  and fix the driving frequency as  $\omega = 2\pi J$ . In the absence of a thermal bath, the dynamics of each spin can be described by the equation of motion (EOM):  $\dot{\mathbf{s}}_i = \mathbf{h}_i^0 \times \mathbf{s}_i$ , where the effective magnetic field  $\mathbf{h}_i^0 = [-V(t)\bar{s}_i^x, 0, h_z]$  with  $\bar{s}_i^x = \sum_{\langle j \rangle} s_j^x + \lambda \sum_{\langle\langle j \rangle\rangle} s_j^x$ .

The periodically driven system is stabilized by introducing dissipation via coupling of each spin to a thermal bath, which can be modeled using methods familiar in the context of Brownian motion. The EOM for each spin is described by a stochastic Landau-Lifshitz-Gilbert equation [41,42]:

$$\dot{\mathbf{s}}_i = \mathbf{h}_i \times \mathbf{s}_i - \eta \mathbf{s}_i \times (\mathbf{s}_i \times \mathbf{h}_i), \quad (4)$$

where  $\eta$  is the dissipation strength fixed as  $\eta = J$  and  $\mathbf{h}_i = \mathbf{h}_i^0 + \boldsymbol{\xi}_i(t)$  is the effective magnetic field, where  $\boldsymbol{\xi}_i(t)$  is a three-dimensional zero-mean ( $\langle \xi_i^\alpha(t) \rangle_\xi = 0$ ) stochastic magnetic field representing a thermal noise. We further assume the local baths around different sites are independent of each other, and the stochastic variables satisfy  $\langle \xi_i^\alpha(t) \xi_j^\beta(t') \rangle_\xi = \mathcal{D}^2 \delta_{\alpha\beta} \delta_{ij} \delta(t - t')$  where  $\alpha, \beta$  are the index of three space dimensions and  $\mathcal{D}$  is the noise strength. The ensemble

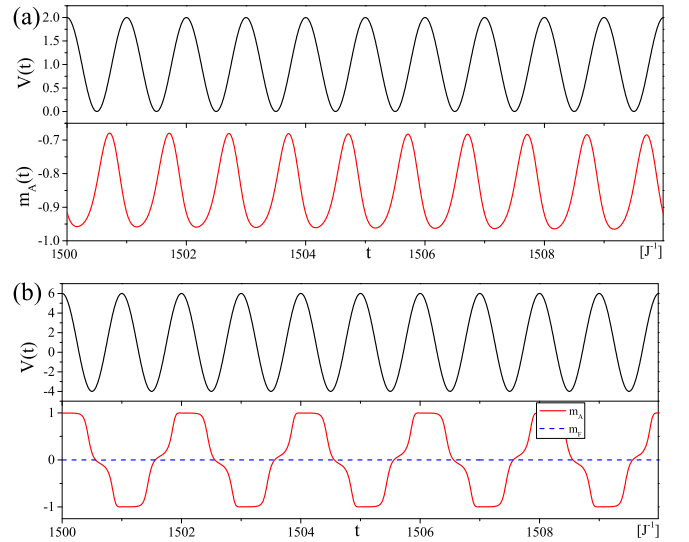


FIG. 2. In the frustration-free case ( $\lambda = 0$ ), (a) long-time dynamics of AFM order parameter  $m_A(t)$  with a weak driving ( $J' = J$ ) and (b) long-time dynamics of the AFM (red solid) and FM (blue dashed) order parameters  $m_A(t)$  and  $m_F(t)$  with a strong driving ( $J' = 5J$ ). Parameters are chosen as  $L = 120$ ,  $\eta = J$ ,  $\mathcal{D} = 0.01J$ ,  $h_z = 1.5J$ , and  $\omega = 2\pi J$ .

average  $\langle \rangle_\xi$  is over all the noise trajectories. For a thermal bath with temperature  $T$ , the strengths of the dissipation and noise satisfy the fluctuation-dissipation theorem  $\mathcal{D}^2 = 2T\eta$ . We fix  $\mathcal{D} = 0.01J$ , which corresponds to an extremely low temperature and does not play a crucial role here. The high-temperature case is discussed in Sec. V. The stochastic differential Eq. (A1) is discretized by adopting Stratonovich's formula, and solving it by the standard Heun method [43] with a time step of  $\Delta t = 10^{-3}J^{-1}$ . The initial state for each spin is chosen as  $[s_i^x, 0, s_i^z]$ , where  $s_i^x \in [-1, 1]$  is a random number, and  $s_i^z$  is fixed according to  $|\mathbf{s}_i| = 1$ . The system size in our simulation is up to  $L = 120$ . Despite the richness of the dynamical phase diagram of this model, below, we only focus on the dynamical phases with SSB in both space and time.

### III. FRUSTRATION-FREE CASE: AN ANTIFERROMAGNETIC DISCRETE TIME CRYSTAL

We start with a frustration-free case ( $\lambda = 0$ ), where we monitor the magnetization dynamics  $s_i^x(t)$  based on Eq. (A1). Without driving ( $J' = 0$ ), the system will relax to an equilibrium AFM state with a nonzero order parameter  $m_A = \frac{1}{L^2} \sum_i (-1)^{i_x+i_y} s_i^x$ . Figure 2 indicates that such an AFM order also persists in the presence of driving. Figure 2(a) shows that in the weak driving case ( $J' = J$ ) where the coupling is always AFM [ $V(t) \geq 0$ ],  $m_A(t)$  oscillates around a finite value with the same frequency with driving. At strong driving ( $J' = 5J$ ), one can also observe a time-dependent AFM order [Fig. 2(b)]; however, such an AFM state differs from its equilibrium counterpart in two aspects. First, the long-range AFM order is present at any time, even at those time slices with FM coupling [ $V(t) < 0$ ]. By contrast, the FM order parameter  $m_F(t) = \frac{1}{L^2} \sum_i s_i^x(t)$  [the blue dashed line, Fig. 2(b)] vanishes in the whole evolution. Furthermore, different from the

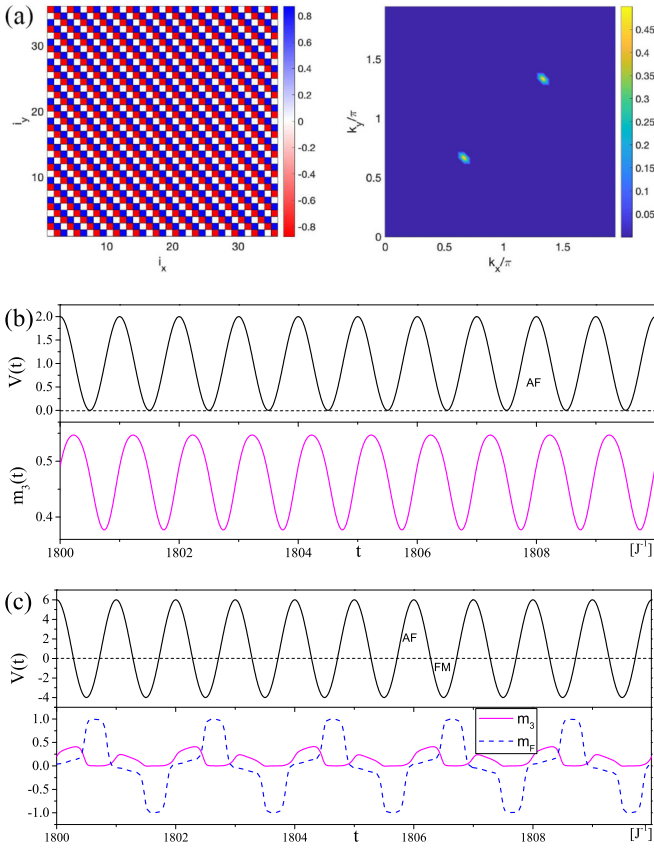


FIG. 3. In a fully frustrated case ( $\lambda = 1$ ), (a) magnetization distribution  $\{s_i^z\}$  of the long-time asymptotic state without driving ( $J' = 0$ ) in a real space (left panel) and its Fourier transformation with the peaks at momenta  $\mathbf{Q}_0$  and  $2\mathbf{Q}_0$  with  $\mathbf{Q}_0 = (\frac{2\pi}{3}, \frac{2\pi}{3})$  (right panel); (b) long-time dynamics of tripartite stripe order parameter  $m_3(t)$  in the weakly driven case ( $J' = J$ ); and (c) long-time dynamics of the tripartite stripe (purple solid) and the FM (blue dashed) order parameters  $m_3(t)$  and  $m_F(t)$  in the strongly driven case ( $J' = 5J$ ).  $L = 120$  except for (a) where  $L = 36$ . Other parameters are chosen the same as those in Fig. 2.

weakly driven case,  $m_A(t)$  oscillates with a period doubling with respect to that of driving, thereby spontaneously breaking

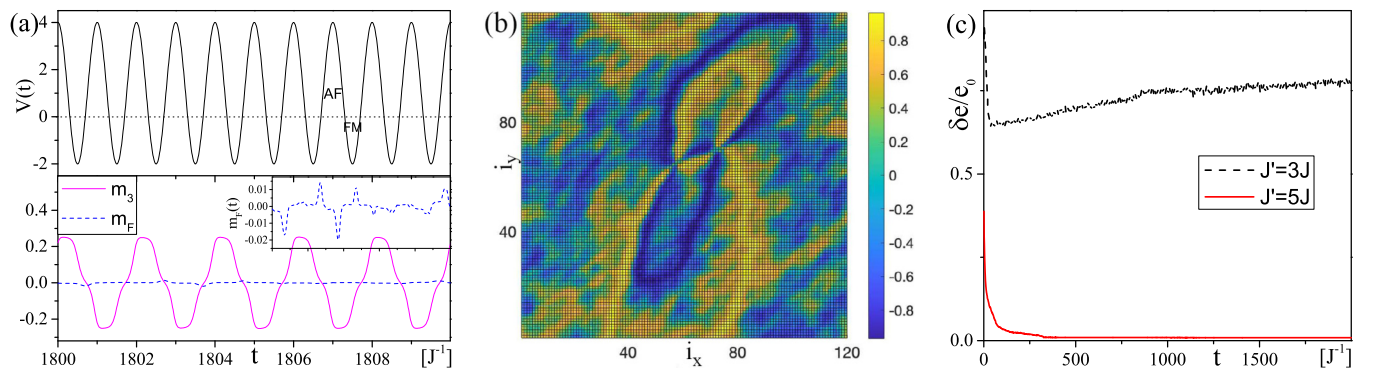


FIG. 4. In a fully frustrated case ( $\lambda = 1$ ) with intermediate driving ( $J' = 3J$ ), (a) long-time dynamics of the tripartite stripe (purple solid) and FM (blue dashed) order parameters  $m_3(t)$  and  $m_F(t)$  [inset magnifies  $m_F(t)$ ]; (b) typical magnetization distribution  $\{s_i^z\}$  in a real space at a time slice with maximal FM coupling; and (c) comparison of the dynamics of excess energy with respect to the perfect FM state at the time slices with maximal FM coupling for the cases with intermediate ( $J' = 3J$ ) and strong ( $J' = 5J$ ) driving. Other parameters are chosen the same as in Fig. 2.

the discrete time translational symmetry from  $\mathbb{Z}$  to  $2\mathbb{Z}$  group. Consequently, such a state simultaneously breaks the space and time translational symmetry; thus it is an AFM discrete time crystal (DTC).

#### IV. FULLY FRUSTRATED CASE: A ZOO OF NONEQUILIBRIUM PHASES OF MATTER

Now we consider a fully frustrated case with  $\lambda = 1$ , where the lattice is equivalent to a triangle lattice. In equilibrium magnetism, frustration works against AFM order. One may wonder whether it plays a similar role of suppressing the aforementioned AFM-DTC order in this nonequilibrium setup. If so, what kinds of space-time structures will emerge once the AFM-DTC is destroyed? Without driving ( $J' = 0$ ), the system will relax toward an equilibrium state close to the ground state of the Hamiltonian (1). The transverse field distinguishes our model from the pure triangle lattice Ising model with extensive ground state degeneracy. Figure 3(a) depicts the steady state magnetization with a tripartite structure and a stripe order along the diagonal direction. This magnetic order is characterized by the order parameter  $m_3(t) = \frac{1}{L^2} \sum_i \sin[\mathbf{Q}_0 \cdot \mathbf{i}] s_i^z(t)$  with  $\mathbf{Q}_0 = (\frac{2\pi}{3}, \frac{2\pi}{3})$ .

The tripartite stripe (TS) order parameter  $m_3(t)$  starts to oscillate once the periodic driving is switched on. With weak driving ( $J' = J$ ), Fig. 3(b) shows that  $m_3(t)$  oscillates around a finite value with a period the same as driving; thus the TS order still persists in this nonequilibrium case. For strong driving ( $J' = 5J$ ),  $V(t)$  alternates between FM and AFM coupling during the evolution, thereby changing the dynamics. Figure 3(c) illustrates that the TS/FM long-range order is built at the time slices with AM/FM coupling. However, this does not mean that the system adiabatically follows the instantaneous ground state of Hamiltonian (1). Instead, it is in a genuine nonequilibrium state because both  $m_3(t)$  and  $m_F(t)$  develop a DTC order in the time domain, indicating that a temporal correlation is dynamically built. In other words, the asymptotic state with strong driving is a space-time crystal that simultaneously breaks the space-time translational symmetry and the  $Z_2$  symmetry in spin space. This space-time crystal differs from the AFM-DTC phase in the  $\lambda = 0$  case, where the FM order is absent even during FM coupling.

The situation is more interesting with intermediate coupling (e.g.,  $J' = 3J$ ). Figure 4(a) illustrates that the TS and the associated DTC orders still persist. However, different from the strongly driven case, the long-range FM order is not built during the whole period. Its order parameter  $m_F(t)$  [dashed blue line, Fig. 4(a)] stochastically oscillates with a small amplitude that decreases with system size, as shown in the Appendix. A typical magnetization configuration  $\{s_i^x\}$  at a time slice with a maximum FM coupling is plotted in Fig. 4(b), which exhibits a wealth of FM domain walls (DWs), and the total magnetization is close to zero. The results show that at intermediate coupling, even though the system builds a short-range FM correlation, it has no time to develop long-range FM order before the coupling turns back to AFM within a driving circle.

To measure the density of the DWs, we define an excess energy density with respect to the perfect FM state as  $\delta e(t) = \frac{1}{L^2} \langle H_s^I(t) \rangle - e_0$ , where  $\langle H_s^I(t) \rangle$  is the instantaneous interaction energy at time  $t$  (we only focus on the time slices with maximal FM coupling) and  $e_0$  is the energy density of a perfect FM state along the  $x$  direction. In Fig. 4(c), for  $J' = 3J$ ,  $\delta e(t)/e_0$  ultimately saturates toward a large value, indicating that it is far from a perfect FM state and the density of DWs does not decay in time. By contrast, for the strong driving case with  $J' = 5J$ , excess energy is very small, indicating that the system could reach an almost perfect FM state at the maximal FM coupling. The difference between the intermediate and strong coupling cases is because the FM coupling duration in the former is shorter than that in the latter. In each driving circle, the FM duration in the case of intermediate driving is not long enough for the system to build up long-range FM correlation.

## V. THE ROLE OF DIFFERENT PARAMETERS IN THE MODEL

Above, we only studied several representative nonequilibrium phases by focusing on special points in the parameter space. In the following, we will systematically examine the role of different parameters of the models in determining the space-time patterns of dynamical phases. The dynamical phase transitions between them have also been studied.

### A. Driving frequency $\omega$

Above, we changed the driving amplitude but fixed the driving frequency as  $\omega = 2\pi J$ . Here, we will exam the role of  $\omega$  in determining the space-time patterns of our model.

In the fast driving limit where  $\omega \gg J$ , the periodic driving oscillates too fast to be followed by the system. In such a high-frequency limit, one can derive an effective time-independent Hamiltonian to describe the stroboscopic dynamics of this periodically driven system, similar to the Floquet analysis in quantum systems, where the effective time-dependent Hamiltonian can be expressed as a expansion in terms of  $1/\omega$ . In the high-frequency limit, the dominant term in the expansion is an average of the Hamiltonian over one period, where  $\frac{1}{T_0} \int_0^{T_0} dt V(t) = J$ ; therefore, the dynamics in this case is similar to the relaxation dynamics in the undriven case ( $J' = 0$ ), where the steady state is a stripe phase with a nonvanishing order parameter  $m_3 = \frac{1}{L^2} \sum_i \sin[\mathbf{Q}_0 \cdot \mathbf{i}] s_i^x(t)$  with  $\mathbf{Q}_0 =$

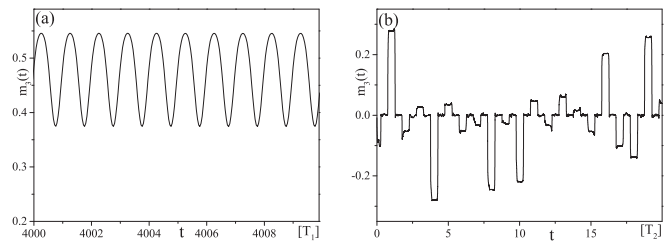


FIG. 5. The dynamics of the 3-period stripe order parameter  $m_3(t)$  in the presence of (a) fast driving with a frequency  $\omega = 8\pi J$  and (b) slow driving with a frequency  $\omega = 0.02\pi$ . The  $x$  axes are plotted in the unit of the corresponding driving periods with  $T_1 = 0.25J^{-1}$  and  $T_2 = 100J^{-1}$ . The parameters are chosen as  $L = 30$ ,  $J' = 5J$ . Other parameters are chosen as  $\eta = J$ ,  $\mathcal{D} = 0.01J$ ,  $\lambda = J$ ,  $h_z = 1.5J$ .

$(\frac{2\pi}{3}, \frac{2\pi}{3})$ . For a large but finite frequency, the order parameter of the stripe phase will oscillate around its equilibrium value with a frequency the same as the driving, as shown in Fig. 5(a), where the frequency is chosen as  $\omega = 8\pi J$ .

In the opposite limit of slow driving, where the period of the driving is much longer than the relaxation time  $\omega \ll \eta$  ( $\eta$  is the dissipation strength), the system has sufficient time to relax; thus at any given time, the system is always close to an equilibrium state. As a consequence, both the FM and the stripe spatial order can be developed depending on the sign of  $V(t)$  in the instantaneous Hamiltonian. However, a thermalization of a system means that it has no memory of the information of its initial state, or the previous states far away from it. As a consequence, for magnetic states with SSB, the system will randomly choose one state among the degenerate manifold with SSB since the interaction does not break the  $Z_2$  symmetry and thus has no preference among the degenerate states. These symmetry-breaking phases at different time slices barely correlate with each other, and thus cannot form a long-range order (DTC) in the time domain, as shown in Fig. 5(b), where the frequency is chosen as  $\omega = 0.02\pi$ .

### B. Frustration $\lambda$

Above, we only studied the unfrustrated ( $\lambda = 0$ ) and fully frustrated ( $\lambda = 1$ ) cases, which exhibit nonequilibrium phases with different SSB. Here, we will systematically study the role of frustration by continuously tuning the frustration strength  $\lambda$ . We focus on strongly driving case ( $J' = 5J$ ). We find that the frustration does not change the DTC nature of the phase, but is crucial in determining the spatial order of the nonequilibrium phases. In general, the magnetic order parameters in these dynamics phases keep oscillating in time; therefore, to characterize their strength, we need to derive a time-independent order parameter. For instance, for the FM order parameter  $m_F(t)$ , we choose those time slices with  $t = t_n^F$  when  $m_F(t)$  reach its  $n$ th maximum, and perform the average over them to derive a time-independent order parameter  $m_F = \langle m_3(t_n^F) \rangle$ , and use it to characterize the strength of the FM order parameter in these dynamics phases.

We plot the time-independent AFM, FM, and tripartite stripe order parameters  $m_A$ ,  $m_F$ , and  $m_3$  as a function of  $\lambda$  in Fig. 6(a), from which we can find that for a small frustration, the AFM-DTC order persist until  $\lambda = 0.68$ , where

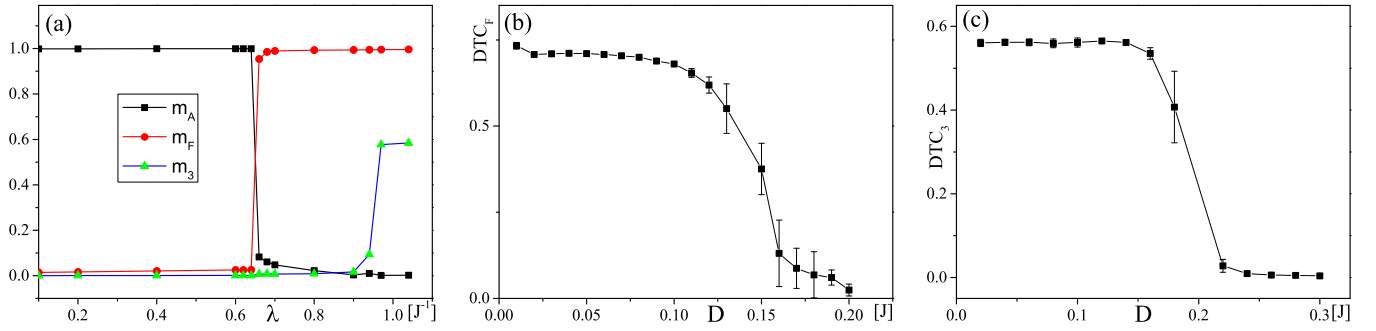


FIG. 6. (a) The time-independent AFM ( $m_A$ ), FM ( $m_F$ ), and tripartite stripe ( $m_3$ ) order parameters as a function of frustration strength  $\lambda$  with  $J' = 5J$  and  $\mathcal{D} = 0.01J$ . (b) In the strongly driven case ( $J' = 5J$ ), the DTC order parameter corresponding to the FM order as a function of noise strength  $\mathcal{D}$ . (c) In the intermediate driven case ( $J' = 3J$ ), the DTC order parameter corresponding to the 3-period stripe order as a function of noise strength  $\mathcal{D}$ .  $\lambda = J$  for (b) and (c). Other parameters are chosen as  $L = 30$ ,  $\eta = J$ ,  $h_z = 1.5J$ ,  $\omega = 2\pi$ .

the AFM order gives way to a FM order via a first-order phase transition. For a frustration within the regime  $\lambda \in [0.68, 0.9]$ , one can find an intermediate phase where the long-range FM order has been built up in the duration of FM coupling, while there is no long-range tripartite stripe order during the AFM coupling. In other words, frustration suppresses the AFM order even in this nonequilibrium driven case, while it facilitates the FM orders, since in the duration with FM coupling [ $V(t) < 0$ ], the next-nearest-neighboring coupling no longer leads to “frustration”; instead it increases the effective FM coupling. When the frustration further increases, the system experiences another first-order dynamical phase transition at  $\lambda = 0.9$  characterized by the sudden onset of the tripartite stripe order, and the system enters a dynamics phase oscillating between the states with long-range FM and tripartite stripe orders, which has been discussed above in the fully frustrated strongly driving case.

### C. Thermal fluctuation $\mathcal{D}$

Above, we focus on the case with weak thermal fluctuation ( $\mathcal{D} = 0.01J$ ), which does not change the nature of the phases with discrete symmetry breaking. However, it is known that the thermal fluctuation works against spontaneous symmetry breaking, and a strong thermal fluctuation could melt the ordered phase and restore the symmetries. Since the space-time crystal phase discussed here simultaneously breaks different symmetries (space and time translational symmetries and  $Z_2$  spin symmetry), one may wonder what is the effect of the thermal fluctuations on these dynamical orders.

As an example, we focus on the DTC order with spontaneous  $Z_2$  symmetry breaking in the time domain, and check whether it is possible for thermal fluctuation to restore this symmetry. Since at low temperature, both  $m_F(t)$  and  $m_3(t)$  exhibit DTC order in the time domain, one needs to distinguish their corresponding DTC order via different order parameters as

$$DTC_a = \frac{2}{t_0} \int_{\frac{t_0}{2}}^{t_0} dt e^{i\pi t} m_a(t) \quad (5)$$

with  $a = F$  or 3 indicating the FM or tripartite stripe order parameter, respectively.  $t_0 = 2000J^{-1}$  is our simulation time and the Fourier transformation is performed over the second half of the full simulation time, during which the system has reached the long-time asymptotic state.

We focus on both cases with intermediate ( $J' = 3J$ ) and strong ( $J' = 5J$ ) driving and study the corresponding DTC order parameters  $DTC_3$  and  $DTC_F$  as a function of  $\mathcal{D}$ . The ensemble average is performed over  $\mathcal{N}$  noise trajectories, with  $\mathcal{N} = 10$ . For the case with strong driving, the DTC order parameter corresponding to the FM order persists until  $\mathcal{D} \approx 0.15J$ , above which the discrete time translational symmetry has been restored [Fig. 6(b)]; however, the DTC order corresponding to the tripartite stripe order is much more fragile; it vanishes for  $\mathcal{D} > 0.03J$  (not shown here). In summary, in the case with strong driving, there exists an intermediate noise regime where the FM-DTC order survives but the stripe-DTC order does not, similar to what happened in the intermediate frustration regime discussed above. In the case with intermediate driving, the long-range FM order has not been built up even in the presence of weak noise and only tripartite stripe order exists. However, different from its counterpart in the strongly driven case, the DTC order corresponding to this tripartite stripe phase in the intermediately driven case is quite robust against thermal fluctuation, as shown in Fig. 6(c). The thermal-fluctuation-induced transitions discussed in these two cases seem to be continuous. However, a precise determination of the position of the phase transition point and the critical properties calls for a finite-size scaling analysis, which will be left to future work.

## VI. SPACE-TIME ORDERS AND PHASE DIAGRAM

### A. Origin of discrete time crystals

The traditional routine to realize a DTC (Ref. [17], for instance) is first considering a noninteracting spin system, where each spin is driven periodically by a time-dependent magnetic field. This simple system could exhibit a trivial period doubling behavior in the presence of a set of fine-tuned parameters of the magnetic field, and thus it is not stable. However, once the interaction is switched on, such a period doubling behavior becomes robust against imperfection of the choice of parameters. In other words, the system is in a stable DTC phase that exists in a finite regime, instead of a special point, in the parameter space. Our model, however, proposed a completely different mechanism to realize DTC. The key difference is that the periodic modulation in our model is not imposed on the external field, but on the interactions. The

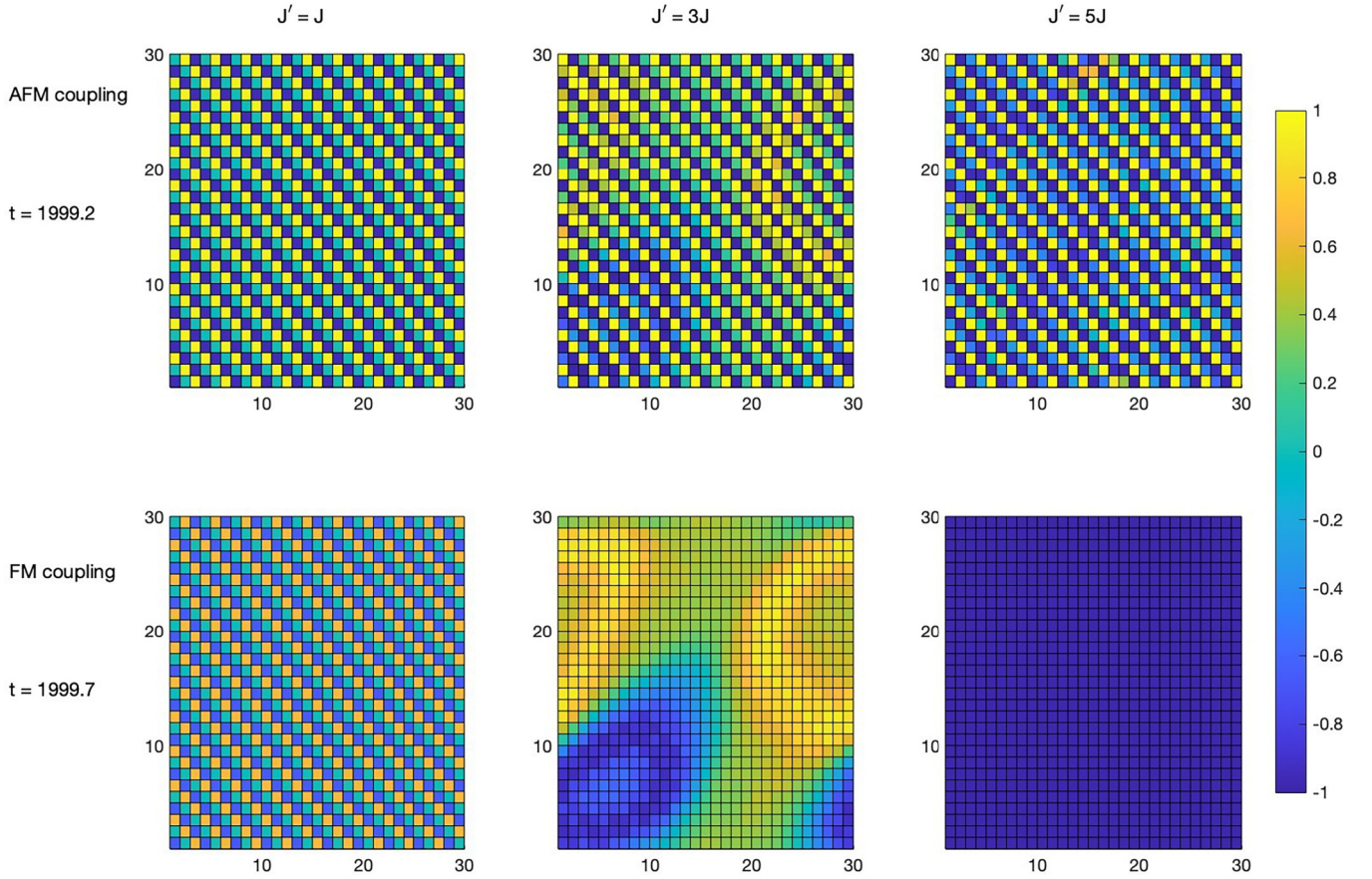


FIG. 7. The snapshots of the spin configuration  $\{s_i^x\}$  at two representative time slices  $t_1$  corresponding to AFM coupling (upper panel) and  $t_2$  corresponding to FM couplings (lower panel) and various  $J'$ . Other parameters are chosen as  $\omega = 2\pi$ ,  $\lambda = 1$ ,  $L = 30$ ,  $D = 0.01J$ , and  $\eta = J$ .

interaction in our model does not play the role of a stabilizer, but a source of DTC.

To understand the nature of this DTC induced by the oscillating interaction, we provide an intuitive picture here. For simplicity, we focus on the frustration-free case where the system exhibits an AFM-DTC order. The interaction Hamiltonian in this case reads as

$$H_I(t) = \sum_{\langle ij \rangle} V(t) s_i^x s_j^x, \quad (6)$$

where  $V(t) \sim \cos \omega t$  is a periodic function (we ignore the constant term for simplicity).  $\langle ij \rangle$  indicates a pair of adjacent lattice sites. We assume both  $s_i^x$  and  $s_j^x$  exhibit periodic oscillations with the same frequency  $\omega'$  and phase  $\phi$ :  $s_i^x \sim \cos[\omega't + \phi]$  and  $s_j^x \sim -\cos[\omega't + \phi]$  (the AFM order indicates that  $s_i^x = -s_j^x$ ). By substituting these simplified formalisms of  $s_i^x$  and  $s_j^x$  into the  $H_I(t)$  and ignoring the constant terms, interaction energy turns to

$$\begin{aligned} H_I(t) &\sim -\cos \omega t \cos(2\omega't + 2\phi) \\ &= -\cos(\omega_- t - 2\phi) - \cos(\omega_+ t + 2\phi), \end{aligned} \quad (7)$$

where  $\omega_- = \omega - 2\omega'$  and  $\omega_+ = \omega + 2\omega'$ . For general values of  $\omega$  and  $\omega'$ ,  $H_I(t)$  is time-dependent, and its long-time average is zero. However if  $\omega'$  takes the value of  $\omega' = \omega/2$  (period doubling),  $\omega_- = 0$  and thus the first term in the right

side of Eq. (7) becomes time independent, while the second term is a rapid oscillating term and thus is not important. Therefore  $H_I(t) \sim -\cos 2\phi$ , which takes its minimum value at two degenerate points  $\phi = 0$  and  $\phi = \pi$ . In a real-time evolution,  $\phi$  can take either of these two minima depending on the initial state, which corresponds to the spontaneously  $Z_2$  temporal translational symmetry breaking in the DTC.

The role of other parameters can also be understood. For instance, the dissipation makes these energy minima become “attractive” as stated by the referee. Because the dynamics is dissipative, these two basins are stable against small perturbation imposed by noise or other imperfections. The transverse field is also necessary to induce nontrivial dynamics of the spin; otherwise the model is only an Ising model and the spin dynamics will be simple precession along the  $z$  direction. In summary, we believe such an oversimplified intuitive picture can capture the essential physics of the periodic doubling in our model.

### B. Snapshots of the spin configurations at time slices with AFM and FM couplings

Now we focus on the spatial magnetic orders, which can be seen more clearly in the snapshots of the spin configurations at different time slices. We first fix the frustration strength  $\lambda = 1$ , and tune the driving amplitude  $J'$ . The snapshots of

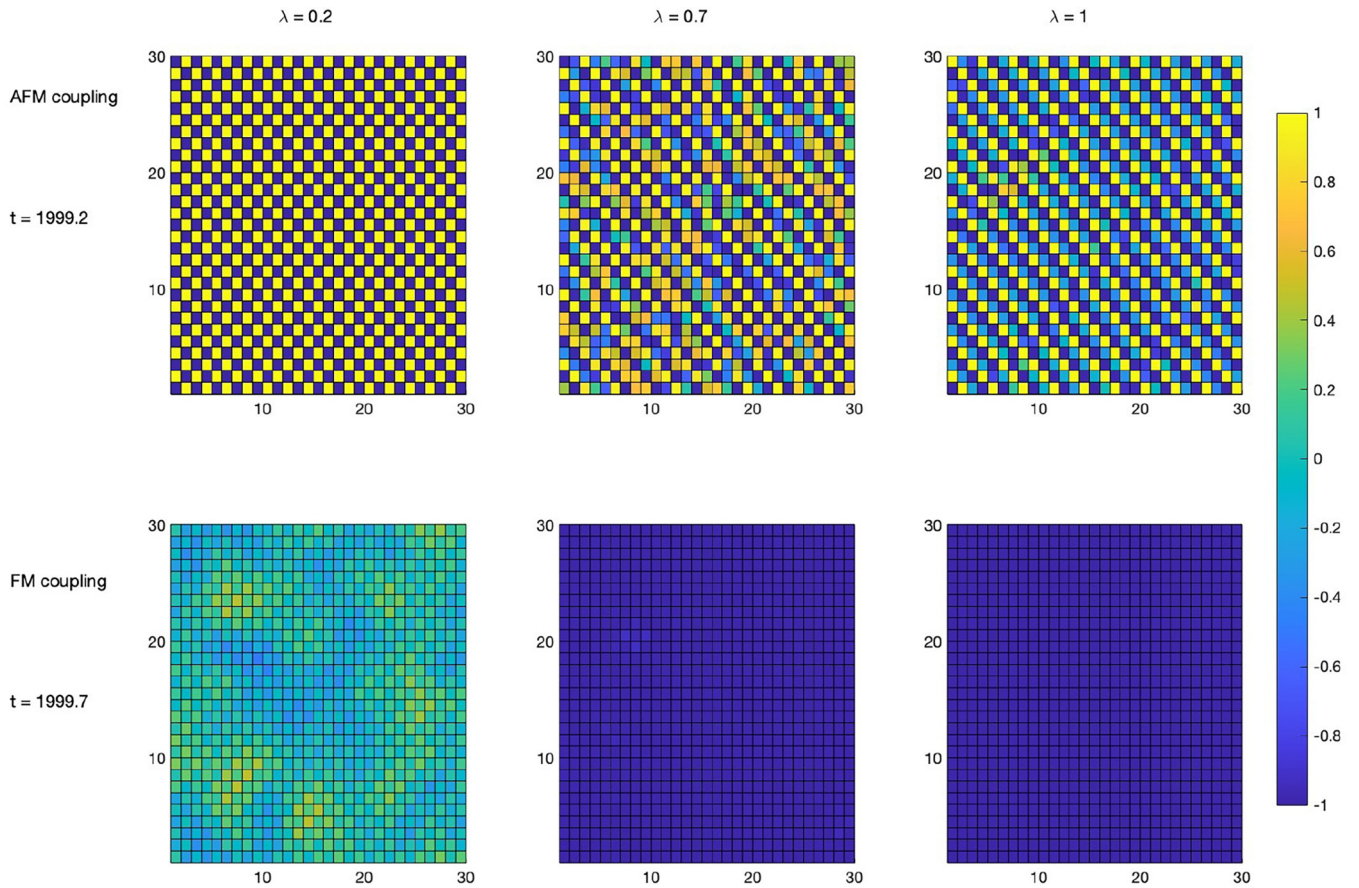


FIG. 8. The snapshots of the spin configuration  $\{s_i^x\}$  at two representative time slices  $t_1$  corresponding to AFM coupling (upper panel) and  $t_2$  corresponding to FM couplings (lower panel) and various  $\lambda$ . Other parameters are chosen as  $\omega = 2\pi$ ,  $J' = 5J$ ,  $L = 30$ ,  $\mathcal{D} = 0.01J$ , and  $\eta = J$ .

the spin configuration  $\{s_i^x\}$  at two representative time slices corresponding to  $V(t = t_1) > 0$  (AFM coupling) and  $V(t = t_2) < 0$  (FM couplings), respectively, and three different  $J'$  are plotted in Fig. 7. Such a real-space visualization indicates that for  $J' = J$ , the system exhibits a tripartite stripe order at both time slices  $t_1$  and  $t_2$ . For  $J' = 3J$ , the tripartite stripe order persists in the presence of AFM coupling. However, at the time slice with FM coupling, the system develops plenty of FM domains while the average magnetization is close to zero, which indicates a short-range FM correlation has been developed, but long-range FM order has not. At  $J = 5J'$ , the system exhibits long-range tripartite stripe order at time slices with AFM coupling, and an almost perfect FM long-range order at the time slices with FM coupling.

Next, we focus on the effect of frustration by fixing the driving amplitude  $J' = 5J$  and increase the frustration strength  $\lambda$  from 0 to 1. We plot the snapshots of  $\{s_i^x\}$  at the AFM and FM coupling time slices with three representative  $\lambda$ . As shown in Fig. 8, for a weak frustration  $\lambda = 0.2$ , the system is in an almost perfect AFM phase at the time slices with AFM coupling, while at FM coupling time slices, the system is in a paramagnetic state without long-range magnetic order. For an intermediate frustration strength  $\lambda = 0.7$ , at the AFM coupling time slice, the AFM order has been completely destroyed by frustration, while the new magnetic order has not been built up yet. On the contrary, at the FM coupling

time slice, the system exhibits an almost perfect FM order, which indicates that in the case with  $\lambda = 0.7$ , the system is in a FM-DTC phase. When we further increase  $\lambda$  into a strongly frustrated regime (e.g.,  $\lambda = 1$ ), the system become an alternating DTC phase, whose magnetic order alternates between the long-range tripartite stripe order and FM order. These results agree with those shown in Fig. 6(a), which indicates that there are three different nonequilibrium phases separated by two phase transitions.

### C. $J'-\omega$ phase diagram

Among all the parameters in our model, three of them are crucial in determining the space-time symmetry breaking: the driving frequency  $\omega$  and amplitude  $J'$  as well as the frustration strength  $\lambda$ . The overall phase diagram of the long-time asymptotic behavior is extremely rich and complex. We first focus on the  $J'-\omega$  phase diagram with a fixed  $\lambda = 1$  for simplicity. As shown in Fig. 9, there are several different dynamics phases within the parameter regime we considered. The synchronized stripe phase indicates the system exhibits a tripartite stripe order whose order parameter oscillates at the same period with the driving. The stripe-DTC phase spontaneously breaks the  $Z_2$  time translational symmetry, and exhibits the tripartite stripe order at the time slices with AFM coupling, while at the time slices with FM coupling, there is no long-range mag-

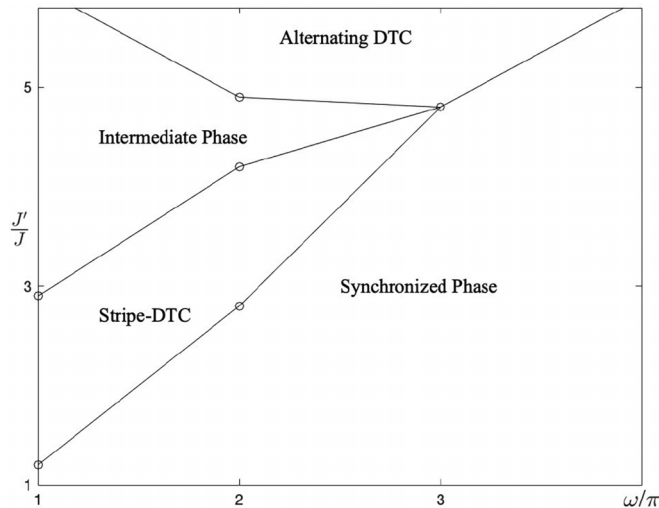


FIG. 9. The phase diagram of the long-time asymptotic dynamics in terms of the driven amplitude  $J'$  and frequency  $\omega$ . Other parameters are chosen as  $\lambda = 1$ ,  $L = 30$ ,  $\mathcal{D} = 0.01J$ , and  $\eta = J$ .

netic order. In the alternating-DTC phase, the system not only breaks the  $Z_2$  time translational symmetry, but also exhibits an alternating tripartite stripe order and FM long-range order at the time slices with AFM and FM coupling, respectively. These three phases have been discussed above. The phase which has not been mentioned above is the intermediate phase between the stripe-DTC and the alternating DTC phases. As shown in Fig. 10, this phase exhibits neither the DTC order in the time domain, nor long-range magnetic order in space. This phase resembles the high-temperature phase in our model (the order parameter is a small but finite value due to the finite-size effect). Further including another parameter  $\lambda$  significantly complicates the phase diagram. For a fixed  $\omega = 2\pi$  and  $J' = 5J$ , the phase diagram in terms of  $\lambda$  has been discussed Fig. 6(a). In the intermediate frustrated regime, there

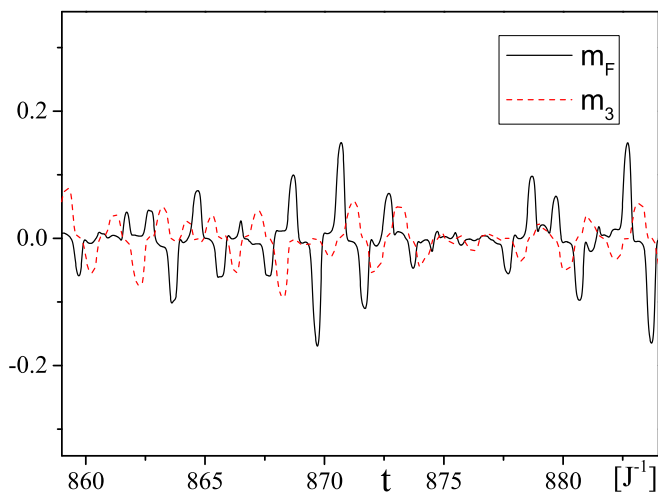


FIG. 10. Dynamics of the FM and tripartite stripe order parameters  $m_F$  and  $m_3$  in the intermediate phase with  $J' = 4.3J$ . Other parameters are chosen as  $\omega = 2\pi$ ,  $\lambda = 1$ ,  $L = 30$ ,  $\mathcal{D} = 0.01J$ , and  $\eta = J$ .

exists a new phase (FM-DTC phase), which only exhibits FM order instead of tripartite stripe order during the time evolution. Also, outside the parameter regime of the phase diagram in Fig. 9, there also exist other dynamical phases. For instance, for an extremely small  $\omega$ , the system exhibits both FM and tripartite stripe long-range order in space at different time slices; however, there is no DTC order in the time domain as shown in Fig. 5(b).

## VII. EXPERIMENTAL REALIZATION OF THE SPACE-TIME CRYSTALS

Even though we studied a classical model which takes an advantage in numerical simulations, the proposed model is difficult to be realized in natural magnetic systems. It requires a time-dependent modulation of the interaction strength, which can be realized using magnetophononics [44–46] although the tunable coupling regime therein is small, and corresponds to a weak driving regime in our model ( $J' < J$ ). The dynamical modulated interaction can also be accessible in synthetic quantum systems. It has been realized that the origin of DTC may not crucially depend on the quantum or classical feature of the interacting systems [35,38–40]. In addition, our model is a 2D system where a long-range order with discrete SSB is supposed to be robust against weak quantum or thermal fluctuations. We therefore expect that the space-time crystals predicted in our classical model can also be observed in synthetic quantum systems like the quantum circuit and cavity QED systems, where the interaction strength can be dynamically modified.

## VIII. CONCLUSION AND OUTLOOK

In this work, we study a nonequilibrium magnetic system with alternate FM and AFM couplings. Introducing frustration into such a driven-dissipative system gives rise to plenty of nonequilibrium phases with SSB in both space and time. Future developments will include the generalization of these results to models with different lattice and spin symmetries. For instance, in other geometric frustrated lattices (e.g., kagome or pyrochlore), one may expect nonequilibrium phases with other magnetic patterns (e.g., nematic or spin ice) and temporal orders (e.g., algebraic temporal correlation [47]) in time. A more exciting possibility is the realization of nonequilibrium states with intertwined space-time symmetries that cannot be decomposed into a direct product of spatial and temporal symmetries [48,49]. As for the spin symmetry, the Hamiltonian (1) preserves the Ising symmetry; generalizing the spin symmetry to continuous ones [e.g.,  $U(1)$ ] may lead to intriguing nonequilibrium phenomena (e.g., a Berezinskii-Kosterlitz-Thouless-like phase transition in such a driven-dissipative system, where the traditional binding-unbinding picture of a vortex [50] may be modified in the context of nonequilibrium physics [51]).

## ACKNOWLEDGMENTS

This work is supported by the National Key Research and Development Program of China (Grant No. 2020YFA0309000), NSFC of China (Grant No. 12174251),

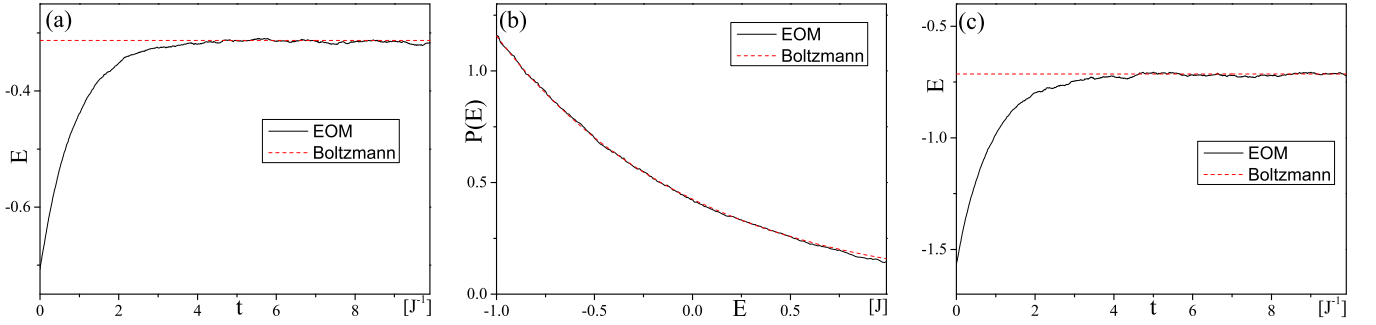


FIG. 11. Relaxation dynamics predicted by Eq. (A1) in the absence of driving. (a) The dynamics of the energy for a single spin model predicted by the EOM (A1), whose long-time asymptotic value approaches that predicted by the statistical ensemble average; (b) the distribution of energy predicted by the EOM (A1), which agrees very well with the Boltzmann distribution. (c) The dynamics of the energy for a two-spin model predicted by the EOM (A1) and the value predicted by statistical ensemble average (red dashed line). The parameters are chosen as  $h_x = J$ ,  $\eta = J$ , and the temperature  $T = J$ .

Natural Science Foundation of Shanghai (Grant No. 22ZR142830), and Shanghai Municipal Science and Technology Major Project (Grant No. 2019SHZDZX01).

## APPENDIX: DETAILS ABOUT THE NUMERICAL SIMULATION

### 1. Heun algorithm

Here, we first derive the discrete formalism of the stochastic Landau-Lifshitz-Gilbert (LLG) equation based on Stratonovich's formula, then formulate the Heun algorithm to solve this stochastic differential equation (SDE). A stochastic LLG equation reads

$$\dot{\mathbf{s}}_i = \frac{1}{\eta^2 + 1} [\mathbf{h}_i \times \mathbf{s}_i - \eta \mathbf{s}_i \times (\mathbf{s}_i \times \mathbf{h}_i)], \quad (\text{A1})$$

where  $\mathbf{s}_i$  is a unit vector.  $\mathbf{h}_i(t) = \mathbf{h}_i^0(t) + \tilde{\mathbf{h}}_i^T(t)$  is the effective magnetic field.  $\mathbf{h}_i^0(t)$  comes from the interaction between spin  $i$  and its neighbors.  $\tilde{\mathbf{h}}_i^T(t)$  is a three-dimensional random magnetic field representing the thermal noise, which satisfies

$$\langle h_i^{T\alpha}(t) \rangle_{\xi} = 0, \quad (\text{A2})$$

$$\langle h_i^{T\alpha}(t) h_j^{T\beta}(t') \rangle_{\xi} = \mathcal{D}^2 \delta_{\alpha\beta} \delta_{ij} \delta(t - t'), \quad (\text{A3})$$

where  $\alpha, \beta$  are the index of three spatial dimensions and  $\mathcal{D}$  is the strength of the noise.  $\langle \rangle_{\xi}$  is the ensemble average over all the trajectories of noises. According to the fluctuation-dissipation theorem, the strength of the thermal noise and the dissipation satisfies the relation

$$\mathcal{D}^2 = 2T\eta. \quad (\text{A4})$$

To solve this SDE numerically, we first discretize the time with the time step of  $\Delta t$ . Let the spin configuration in the  $m$ th time step ( $t_m = m\Delta t$ ) be  $\{\mathbf{s}_i^m\}$ ; the calculation of  $\{\mathbf{s}_i^{m+1}\}$  can be divided into two steps in the Heun algorithm.

In the first step, we derive an intermediate spin configuration  $\{\tilde{\mathbf{s}}_i^{m+1}\}$ :

$$\tilde{\mathbf{s}}_i^{m+1} = \mathbf{s}_i^m + \frac{1}{\eta^2 + 1} [\mathbf{h}_i^m \times \mathbf{s}_i^m - \lambda \mathbf{s}_i^m \times (\mathbf{s}_i^m \times \mathbf{h}_i^m)] \Delta t \quad (\text{A5})$$

with  $\mathbf{h}_i^m = \mathbf{h}_{i,m}^0 + \tilde{\mathbf{h}}_{i,m}^T$ , where  $\mathbf{h}_{i,m}^0 = \mathbf{h}_i^0(t_m)$  and  $\tilde{\mathbf{h}}_{i,m}^T$  is a stochastic magnetic field satisfying

$$\tilde{h}_{i,m}^{T\alpha} = \frac{\mathcal{D}}{\sqrt{\Delta t}} \xi_{i,m}^{\alpha}, \quad (\text{A6})$$

where  $\xi_i^{\alpha}$  is a random number satisfying the Gaussian distribution with zero mean and unit variance:  $\langle \xi_i^{\alpha} \rangle_{\xi} = 0$ ,  $\langle (\xi_i^{\alpha})^2 \rangle_{\xi} = 1$ .

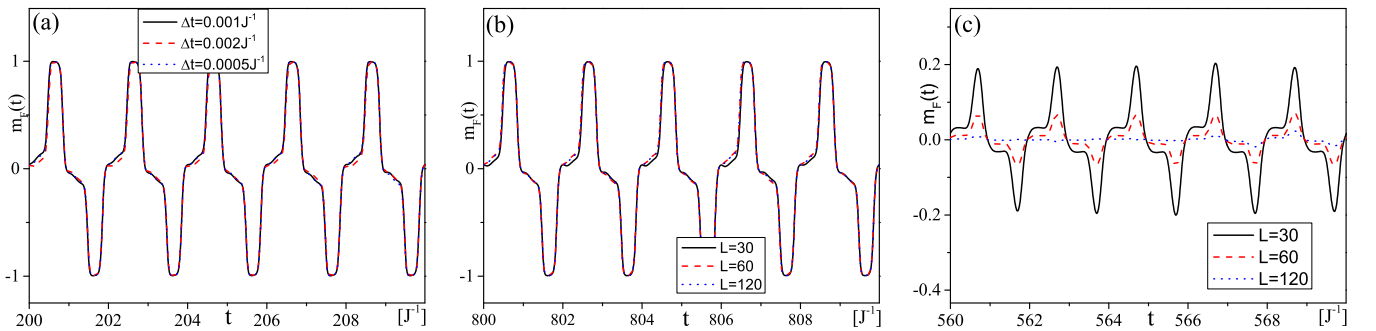


FIG. 12. (a) Comparison between the dynamics of FM order parameter  $m_F(t)$  with different  $\Delta t$  with  $J' = 5J, L = 30$ . Comparison between the dynamics of FM order parameter  $m_F(t)$  with different system size  $L$  (b) in the strong driving case ( $J' = 5J$ ) and (c) in the intermediate driving case ( $J' = 3J$ ). Other parameters are chosen as  $\eta = J, \mathcal{D} = 0.01J, \lambda = J, h_z = 1.5J, \omega = 2\pi$ .

In the Heun algorithm,  $\mathbf{s}_i$  at the  $(m + 1)$ th time step can be expressed as

$$\begin{aligned} \mathbf{s}_i^{m+1} = & \mathbf{s}_i^m + \frac{\Delta t}{2} [\mathbf{h}_i^m \times \mathbf{s}_i^m - \lambda \mathbf{s}_i^m \times (\mathbf{s}_i^m \times \mathbf{h}_i^m) \\ & + \tilde{\mathbf{h}}_i^{m+1} \times \tilde{\mathbf{s}}_i^{m+1} - \lambda \tilde{\mathbf{s}}_i^{m+1} \times (\tilde{\mathbf{s}}_i^{m+1} \times \tilde{\mathbf{h}}_i^{m+1})], \end{aligned} \quad (\text{A7})$$

where  $\tilde{\mathbf{s}}_i^{m+1}$  has been defined in Eq. (A5), and  $\tilde{\mathbf{h}}_i^{m+1} = \mathbf{h}_{i,m+1}^0 + \tilde{\mathbf{h}}_{i,m}^T$ .

## 2. Benchmark: Spin models without driving

It is known that once a system couples to a heat bath, it will finally relax to a thermodynamical equilibrium state at the same temperature of the bath, irrespective of its initial state. To verify the validity of the EOM (A1), we consider two simple spin models as benchmarks, which show that the long-time asymptotic state derived by EOM (A1) is indeed the thermodynamic equilibrium state at a temperature determined by Eq. (A4).

The first model we consider is a single spin model with the Hamiltonian

$$H_1^s = h_z s_z^s. \quad (\text{A8})$$

By solving EOM (A1) using the Heun algorithm, we can find that the energy of the system  $E(t) = \langle H(t) \rangle$  quickly relaxes to a value with small statistical fluctuation. According to the statistical physics, for a thermodynamical equilibrium state, the long-time average of the system energy is supposed to be the same with the value predicted by the statistical ensemble, which is

$$E_s = \frac{1}{Z} \int_0^\pi \sin \theta d\theta (h_z \cos \theta) e^{-\beta h_z \cos \theta}, \quad (\text{A9})$$

where  $\theta$  is the angle between the spin vector and  $z$  axis, and  $Z = \int_0^\pi \sin \theta d\theta e^{-\beta h_z \cos \theta}$  is the partition function. As shown in Fig. 11(a), the time-averaged value of  $\langle H(t) \rangle$  agrees very well with the ensemble-averaged value  $E_s$  within the statistical error. In addition, one can study the statistical distribution of  $E(t)$  during the long-time dynamics;  $P(E)$  agrees very well with the Boltzmann distribution, as shown in Fig. 11(b).

We also check a two-spin model with the Hamiltonian

$$H_s^2 = J s_1^x s_2^x + h_z (s_1^z + s_2^z). \quad (\text{A10})$$

We study the evolution of the system, and focus on its energy. As shown in Fig. 11(c), in the long-time limit, the system energy will approach the value predicted by a canonical ensemble accompanied by small statistical fluctuations.

## 3. Convergence of numerical results

*Finite  $\Delta t$ .* Throughout the main text, we chose a discrete time step of  $\Delta t = 10^{-3} J^{-1}$ . For a stochastic differential equation, the choice of  $\Delta t$  is more subtle than that in the deterministic equation since the random variable depends on  $\Delta t$  as shown in Eq. (A6). To examine the convergence of our result with  $\Delta t$ , we choose different  $\Delta t J = 2 \times 10^{-3}$ ,  $10^{-3}$ , and  $5 \times 10^{-4}$ , and compare their results. As shown in Fig. 12(a), the results with different  $\Delta t$  agree with each other very well, which indicates that the  $\Delta t$  chosen in our simulation is suffi-

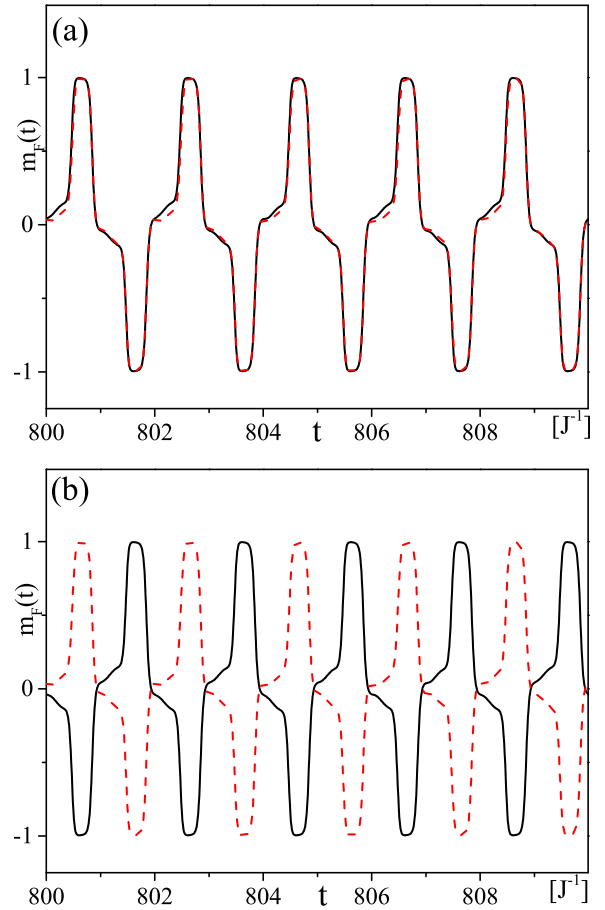


FIG. 13. Comparison between the dynamics of FM order parameter  $m_F(t)$  with (a) different noise trajectories and (b) different initial states with  $J' = 5J$  and  $L = 30$ . Other parameters are chosen the same as in Fig. 12.

ciently small, thus enabling us to ignore the errors induced by the discretization of time.

*Finite  $L$ .* In the main text, the system we simulated is up to a system size with  $L = 120$ . One needs to check the system size dependence of our results. For an ordered phase [e.g., the DTC phase with strong driving ( $J' = 5J$ )], as shown in Fig. 12(b), the deviation between the results with  $L = 30$ , 60, and 120 is pretty small. However, in the intermediate driving regime without true long-range ferromagnetic (FM) order, the FM order parameter  $m_F(t)$  strongly depends on the system size. As shown in Fig. 12(c), the amplitude of  $m_F(t)$  significantly decreases with  $L$ . This is due to the fact that in the presence of intermediate driving, the long-range FM order has not been built up during the FM coupling. Instead, the system is spontaneously separated into different FM domains, and the overall FM order parameter is a summation of the magnetization of them. Within each FM domain, the magnetization oscillates as a DTC, but the phases of these DTCs are not coherent, and thus the magnetizations in different domains at a given time cancel with each other. As a consequence, the overall FM order parameter decreases with the system size.

The different finite-size dependence of the FM order parameter between the strong and intermediate driving can be

considered as the signature of the different dynamical phases with long-range and short-range FM orders, respectively. In addition, the finite-size effect is supposed to be important near the dynamical critical points, which is an important issue but not addressed in this work.

*Noise trajectories.* In principle, one needs to simulate over different noise trajectories and perform the ensemble average over them. However, in our simulation, we only randomly choose one noise trajectory for each set of parameters. This is because we are only interested in the situation with weak noise ( $\mathcal{D} = 0.01J$ ), where a small thermal fluctuation does not change the nature of the phases with discrete symmetry breaking [see the comparison between the dynamics over two different noise trajectories in Fig. 13(a)]. However, for some special initial states, it is possible that the system could be trapped into a metastable state if there are no thermal fluctuations. The role of noise in our simulation is to thermally activate the system and make it escape from the metastable

state after a sufficiently long time and enter the genuine asymptotic long-time states discussed in the main text.

*Initial states.* In our simulation, we start from a spatially inhomogeneous random initial state: for each site, we choose its initial state as  $s_i^0 = [s_i^x, 0, s_i^z]$ , where  $s_i^x$  is a random number different from site to site and uniformly distributed within  $[-1, 1]$ ; the  $z$  component of the spin is chosen correspondingly as  $s_i^z = \sqrt{1 - [s_i^x]^2}$ . Since we focus on the nonequilibrium phases with spontaneously symmetry breaking, it is well known that in this case, the final state is supposed to be highly sensitive to the initial state. This statement does not only work for equilibrium phases (FM or AFM order), but also for nonequilibrium phases. For instance, for a DTC phase with spontaneously  $Z_2$  time translational symmetry breaking, as shown in Fig. 13(b), starting from different initial states, the system could finally fall into either one of the  $Z_2$  breaking phases, each of which is related with the other by a half-period shift in time domain.

- 
- [1] M. Mezard, G. Parisi, and M. Virasoro, *Spin Glass Theory and Beyond: An Introduction to the Replica Method and Its Applications* (World Scientific, Singapore, 1986).
- [2] C. Lacroix, P. Mendels, and F. Mila, *Introduction to Frustrated Magnetism: Materials, Experiments, Theory* (Springer, Heidelberg, 2011).
- [3] J. Villain, *Z. Phys. B* **33**, 31 (1979).
- [4] C. L. Henley, *J. Appl. Phys.* **61**, 3962 (1987).
- [5] A. Chubukov, *Phys. Rev. Lett.* **69**, 832 (1992).
- [6] P. W. Anderson, *Mater. Res. Bull.* **8**, 153 (1973).
- [7] Y. Wan and R. Moessner, *Phys. Rev. Lett.* **119**, 167203 (2017).
- [8] Y. Wan and R. Moessner, *Phys. Rev. B* **98**, 184432 (2018).
- [9] N. Bittner, D. Golež, M. Eckstein, and P. Werner, *Phys. Rev. B* **102**, 235169 (2020).
- [10] H.-K. Jin, A. Pizzi, and J. Knolle, *Phys. Rev. B* **106**, 144312 (2022).
- [11] R. Hanai, [arXiv:2208.08577](https://arxiv.org/abs/2208.08577).
- [12] M. Cross and H. Greenside, *Pattern Formation and Dynamics in Nonequilibrium Systems* (Cambridge University Press, Cambridge, 2009).
- [13] F. Wilczek, *Phys. Rev. Lett.* **109**, 160401 (2012).
- [14] P. Bruno, *Phys. Rev. Lett.* **111**, 070402 (2013).
- [15] H. Watanabe and M. Oshikawa, *Phys. Rev. Lett.* **114**, 251603 (2015).
- [16] K. Sacha, *Phys. Rev. A* **91**, 033617 (2015).
- [17] D. V. Else, B. Bauer, and C. Nayak, *Phys. Rev. Lett.* **117**, 090402 (2016).
- [18] V. Khemani, A. Lazarides, R. Moessner, and S. L. Sondhi, *Phys. Rev. Lett.* **116**, 250401 (2016).
- [19] N. Y. Yao, A. C. Potter, I.-D. Potirniche, and A. Vishwanath, *Phys. Rev. Lett.* **118**, 030401 (2017).
- [20] S. Choi, R. Landig, G. Kucsko, H. Zhou, J. Isoya, F. Jelezko, S. Onoda, H. Sumiya, V. Khemani, C. von Keyserlingk *et al.*, *Nature (London)* **543**, 221 (2017).
- [21] J. Zhang, P. W. Hess, A. Kyprianidis, P. Becker, A. Lee, J. Smith, G. Pagano, I.-D. Potirniche, A. C. Potter, A. Vishwanath *et al.*, *Nature (London)* **543**, 217 (2017).
- [22] S. Autti, V. B. Eltsov, and G. E. Volovik, *Phys. Rev. Lett.* **120**, 215301 (2018).
- [23] J. Smits, L. Liao, H. T. C. Stoof, and P. van der Straten, *Phys. Rev. Lett.* **121**, 185301 (2018).
- [24] N. Träger, P. Gruszecki, F. Lisiecki, F. Groß, J. Förster, M. Weigand, H. Głowiński, P. Kuświk, J. Dubowik, G. Schütz *et al.*, *Phys. Rev. Lett.* **126**, 057201 (2021).
- [25] X. Yang and Z. Cai, *Phys. Rev. Lett.* **126**, 020602 (2021).
- [26] J. N. Stehouwer, H. T. C. Stoof, J. Smits, and P. van der Straten, *Phys. Rev. A* **104**, 043324 (2021).
- [27] X. Mi, M. Ippoliti, C. Quintana, A. Greene, Z. Chen, J. Gross, F. Arute, K. Arya, J. Atalaya, R. Babbush *et al.*, *Nature (London)* **601**, 531 (2022).
- [28] P. Frey and S. Rachel, *Sci. Adv.* **8**, 7652 (2022).
- [29] P. Kongkhambut, J. Skulte, L. Mathey, J. G. Cosme, A. Hemmerich, and H. Kessler, *Science* **377**, 670 (2022).
- [30] A. Pizzi, A. Nunnenkamp, and J. Knolle, *Nat. Commun.* **12**, 1061 (2021).
- [31] Q. Zhuang, F. Machado, N. Y. Yao, and M. P. Zaletel, [arXiv:2110.00585](https://arxiv.org/abs/2110.00585).
- [32] M. McGinley, S. Roy, and S. A. Parameswaran, *Phys. Rev. Lett.* **129**, 090404 (2022).
- [33] M. Yue, X. Yang, and Z. Cai, *Phys. Rev. B* **105**, L100303 (2022).
- [34] C. Lupo and C. Weber, *Phys. Rev. B* **100**, 195431 (2019).
- [35] N. Y. Yao, C. Nayak, L. Balents, and M. P. Zaletel, *Nat. Phys.* **16**, 438 (2020).
- [36] F. M. Gabbetta, F. Carollo, A. Lazarides, I. Lesanovsky, and J. P. Garrahan, *Phys. Rev. E* **100**, 060105(R) (2019).
- [37] R. Khassseh, R. Fazio, S. Ruffo, and A. Russomanno, *Phys. Rev. Lett.* **123**, 184301 (2019).
- [38] R. Hurtado-Gutiérrez, F. Carollo, C. Pérez-Espigares, and P. I. Hurtado, *Phys. Rev. Lett.* **125**, 160601 (2020).
- [39] B. Ye, F. Machado, and N. Y. Yao, *Phys. Rev. Lett.* **127**, 140603 (2021).
- [40] A. Pizzi, A. Nunnenkamp, and J. Knolle, *Phys. Rev. Lett.* **127**, 140602 (2021).

- [41] W. F. Brown, *Phys. Rev.* **130**, 1677 (1963).
- [42] P.-W. Ma, S. L. Dudarev, A. A. Semenov, and C. H. Woo, *Phys. Rev. E* **82**, 031111 (2010).
- [43] S. Ament, N. Rangarajan, A. Parthasarathy, and S. Rakheja, [arXiv:1607.04596](https://arxiv.org/abs/1607.04596).
- [44] M. Yarmohammadi, C. Meyer, B. Fauseweh, B. Normand, and G. S. Uhrig, *Phys. Rev. B* **103**, 045132 (2021).
- [45] K. Deltenre, D. Bossini, F. B. Anders, and G. S. Uhrig, *Phys. Rev. B* **104**, 184419 (2021).
- [46] D. Bossini, S. Dal Conte, M. Terschanski, G. Springholz, A. Bonanni, K. Deltenre, F. Anders, G. S. Uhrig, G. Cerullo, and M. Cinchetti, *Phys. Rev. B* **104**, 224424 (2021).
- [47] N. Prokofev and B. Svistunov, *J. Exp. Theor. Phys.* **127**, 860 (2018).
- [48] S. Xu and C. Wu, *Phys. Rev. Lett.* **120**, 096401 (2018).
- [49] Q. Gao and Q. Niu, *Phys. Rev. Lett.* **127**, 036401 (2021).
- [50] J. M. Kosterlitz and D. J. Thouless, *J. Phys. C* **6**, 1181 (1973).
- [51] E. Altman, L. M. Sieberer, L. Chen, S. Diehl, and J. Toner, *Phys. Rev. X* **5**, 011017 (2015).